12-2015

The Gaussian Approximation to Multiple-Access Interference in the Evaluation of the Performance of a Communication System with Convolutional Coding and Viterbi Decoding

Snigdhaswin Kar
Clemson University

The Gaussian Approximation to Multiple-Access Interference in the Evaluation of the Performance of a Communication System with Convolutional Coding and Viterbi Decoding

---

A Thesis
Presented to
the Graduate School of
Clemson University

In Partial Fulfillment
of the Requirements for the Degree
Master of Science
Electrical Engineering

---

by
Snigdhaswin Kar
December 2015

Accepted by:
Dr. Daniel L. Noneaker, Committee Chair
Dr. Harlan B. Russell
Dr. Kuang-Ching Wang

Abstract

The standard Gaussian approximation is extended to the performance analysis of direct-sequence code-division multiple-access (DS-CDMA) systems using binary convolutional coding, quaternary modulation with quaternary direct-sequence spreading and Viterbi decoding. Using the standard Gaussian approximation, the random variables modeling the multiple-access interference in the receiver statistics are replaced by an equivalent additive Gaussian noise term with the same variance as the actual multiple-access interference term. The Gaussian approximation is shown to result in an accurate approximation to the probability of code-word error at the receiver. The accuracy is demonstrated by comparing simulation results for the actual multiple-access system and a model using the standard Gaussian approximation. Both are compared with two previously developed closed-form bounds on the performance: the concave-first-event bound and the concave-integral bound.

Acknowledgments

I would like to express my sincere gratitude to my advisor Dr. Daniel L. Noneaker for his valuable guidance throughout my graduate studies, and his patience in the development of this thesis. His support and in-depth knowledge of the subject have helped me immensely in my research. I would also like to thank Dr. Harlan B. Russell and Dr. Kuang-Ching Wang for serving as members of my committee and for sharing their knowledge and insight. I also thank my colleagues in the Wireless Communication Systems and Networks group for their help during my graduate studies.

I would like to thank my friends for their support and encouragement. I would also like to extend a special thanks to my parents for their guidance and support.

Table of Contents

List of Figures

Chapter 1

Introduction

Direct-sequence spread-spectrum modulation is used in a number of wireless communication networks that support multiple concurrent radio links within the same frequency band in a given area. The most widely known of the networks are the cellular communication networks that employ direct-sequence spread-spectrum multiple-access communications which is referred to as code-division multiple-access (or *CDMA*) communications in that context [1]. A less well known application is in ad hoc packet-radio radio networks [2] which are designed to provide robust digital communication capability in the absence of the fixed infrastructure that is present in a cellular CDMA network.

There is much active research focused on developing improved protocols to support greater data throughput and better quality of service in the highly dynamic environment of an ad hoc packet radio network. The complexity of ad hoc networks is such that Monte Carlo simulation of the networks is a key tool in the research, and high-fidelity simulation requires extensive simulation time or computational resources. Much of the computational burden comes from accurate simulation of the physical-layer communications (channel coding, modulation, demodulation, and decoding) in each link of the radio network. Any technique that reduces the computational burden without sacrificing accuracy in the link simulation is highly desirable.

That is the underlying motivation for the focus of this thesis. Specifically, we con-

sider a single communication link in a multiple-access interference environment and examine the accuracy of a key simplifying approximation to the link characteristics and simple bounds on the link performance. The approximation is the standard Gaussian approximation (SGA), which replaces the terms in the receiver statistics of the link due to multiple-access interference with an "equivalent" additive Gaussian noise term [3]. The closed-form bounds were developed previously [4].

In this thesis, we consider a digital communication system in which the transmitter employs binary convolutional coding, quaternary modulation with quaternary direct-sequence spreading and the receiver employs coherent, soft-decision Viterbi decoding. The received signal is corrupted by additive white Gaussian noise and possibly one or more interfering signals from transmitters using the same transmission format as the desired signal. We consider the performance of the link as measured by the probability of error in the detected code word provided as the output of the Viterbi decoder.

A closed-form expression is developed for the first and second moments of the multiple-access interference terms in the receiver statistics of the system. They serve as the basis for the SGA. The effect of the SGA to multiple-access interference is evaluated by comparing the simulated performance of the system using actual interfering signals with simulation results using the SGA. The performance is also compared with closed-form bounds on the performance which also make use of the SGA. Performance comparisons are provided for several examples of a convolutional encoder and a range of multiple-access interference channels.

In Chapter 2, we introduce the system model and develop the notation used in the subsequent chapters. We discuss the transmitted signals and received signals and their statistical models. The decision statistic is also discussed in this chapter and we define various measures of the quality of the received signal. In Chapter 3, we develop closed-form expressions for the first and second moments of the multiple-access interference terms in the receiver statistics. The effect of the SGA on pairwise error-event probabilities in a soft-decision Viterbi decoder is examined in Chapter 4. Two bounds on the probability

of code-word error are presented in Chapter 5. The accuracy of the approximations is investigated in Chapter 6 for several examples of encoders and channels, and conclusions are presented in Chapter 7.

Chapter 2

System Description

2.1 System Model

We consider a communication system with K transmitted signals using quaternary modulation and quaternary, direct-sequence spreading [3], where each signal represents information from a different source. The system we consider is shown in Figure 2.1. Each

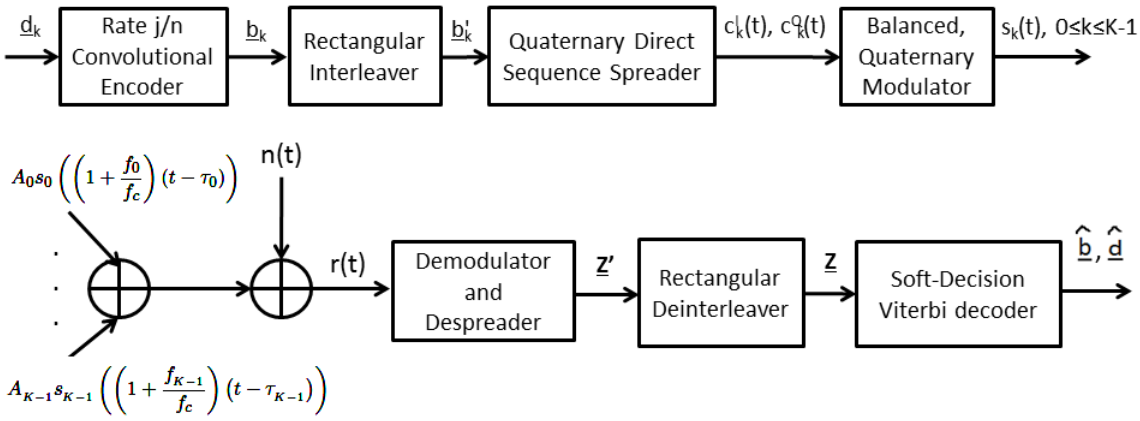

Figure 2.1: System Model.

transmitter uses a rate-j/n binary convolutional encoder of memory order m and a code-symbol interleaver. The transmitted signal passes through a channel characterized by an

additive white Gaussian noise (AWGN) random process and it is corrupted by additive interference from the other transmissions to give the received signal. The receiver converts the received signal to a received word $\underline{Z}$ using a demodulator, a despreader and a deinterleaver. The received word is decoded using soft-decision Viterbi decoding.

2.1.1 Transmitted Signal

The communication system considered in this thesis includes K transmitted signals, $s_k(t)$, $0 \leq k \leq K-1$, and the transmitter for the kth signal is shown in Figure 2.2. The information source at the transmitter generates the sequence of binary information words $\underline{d}_k^{(i)} = (d_{k,ij(L-m)}, ..., d_{k,(i+1)j(L-m)-1})$, $-\infty < i < \infty$. The ith information word is encoded into the code word $\underline{b}_k^{(i)} = (b_{k,inL}, ..., b_{k,(i+1)nL-1})$ using a rate-j/n binary convolutional encoder of memory order m that is given by the generator polynomial G [5]. Each $(L-m)j$-bit information word has mj tail bits appended prior to input into the encoder, which forces the encoder to the all-zeros state at the end of the encoding [5] and results in L encoding time steps per information word. Each code word is interleaved prior to transmission in an rectangular array in which the code symbols are written into the array by rows and read out of the array by columns. The ith interleaved code word is $\underline{b}_k^{(i)'} = (b'_{k,inL}, ..., b'_{k,(i+1)nL-1})$.

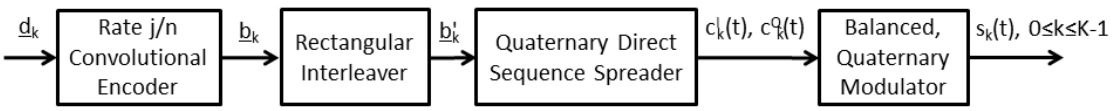

Figure 2.2: Transmitter for kth signal.

The kth transmitted signal, $s_k(t)$, is determined by the sequence of interleaved code words $\{\underline{b}_k^{(i)'}\}$, $-\infty < i < \infty$. The binary code symbols from the kth transmitter form the kth data signal,

$$b'_k(t) = \sum_{i=-\infty}^{\infty} (-1)^{b'_{k,i}} p_T(t - iT) \tag{2.1}$$

where $p_T(t)$ is the unit pulse over [0,T] and T is the bit duration. The kth data signal is spread by inphase and quadrature spreading signals

$$a_k^I(t) = \sum_{l=-\infty}^{\infty} (-1)^{a_{k,l}^I} \psi_c(t - lT_c) \tag{2.2}$$

and

$$a_k^Q(t) = \sum_{l=-\infty}^{\infty} (-1)^{a_{k,l}^Q} \psi_c(t - lT_c) \tag{2.3}$$

respectively, using N chips per code symbol, where the chip waveform $\psi_c(t)$ is time-limited to [0,T_c] and has total energy T_c. The inphase and quadrature binary spreading sequences for the kth transmitted signal are thus $\left\{a_{k,i}^I\right\}$, $-\infty < i < \infty$ and $\left\{a_{k,i}^Q\right\}$, $-\infty < i < \infty$, respectively. The data-modulated spreading inphase and quadrature signals are

$$c_k^I(t) = b_k'(t) a_k^I(t) \tag{2.4}$$

and

$$c_k^Q(t) = b_k'(t) a_k^Q(t), \tag{2.5}$$

respectively. They are modulated onto respective inphase and quadrature sinusoidal carriers. The resulting kth transmitted signal is thus given by

$$s_k(t) = \sqrt{2P_k} c_k^I(t) \cos(2\pi f_c t + \theta_k) + \sqrt{2P_k} c_k^Q(t) \sin(2\pi f_c t + \theta_k) \tag{2.6}$$

where θ_k is the carrier phase angle, f_c is the carrier frequency in Hertz, and P_k is the transmitted power in each of the inphase and quadrature components of the transmitted signal.

2.1.2 Channel

2.1.2.1 Channel Characterization

The transmitted signal $s_0(t)$ passes through an additive channel characterized by the white Gaussian noise random process $n(t)$, and interference from the other $K-1$ transmissions. The channel is shown in Figure 2.3. Each transmitted signal undergoes a

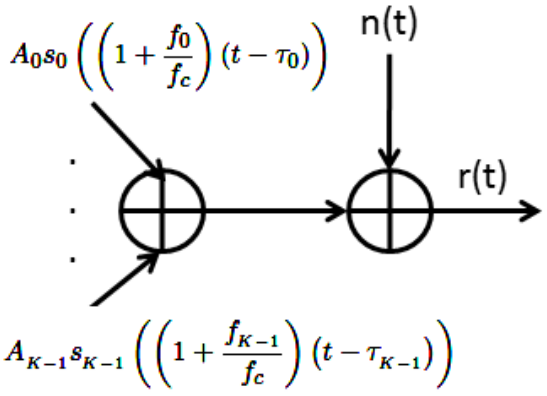

Figure 2.3: Channel.

fixed attenuation, a delay, and a fixed Doppler shift between the transmitter and a receiver that observes the received signal $r(t)$. The channel results in a received signal that is the sum of the attenuated, delayed transmitted signals and $n(t)$. It is thus a multiple-access additive white Gaussian noise (AWGN) channel, and

$$r(t) = \sum_{k=0}^{K-1} A_k s_k \left(\left(1+\frac{f_k}{f_c}\right)(t-\tau_k)\right) + n(t) \tag{2.7}$$

where the magnitude gain in the kth signal at the receiver is A_k, the fixed Doppler shift in the kth signal at the receiver is f_k, and the time delay of the kth signal at the receiver is τ_k. The two-sided power spectral density of $n(t)$ is $N_0/2$.

2.1.2.2 Partial-Time Interference

In general, the channel we consider includes a set of interferers that transmit during part of the transmission time of the desired signal and are idle during the rest of the desired signal's transmission. At a given time during the transmission of the desired signal, either all K-1 interferers are active (in which case the received signal is given by equation (2.7)) or none of the interferers are active (in which case the received signal is given by equation (2.7) with K=1). The fraction of the transmission interval of the desired signal during which the interferers are active is the *interference activity* of the system, which is denoted by ρ. Thus, ρ=0 for a system without multiple-access interference, and ρ=1 for a system with multiple-access interference present throughout the desired transmission. Simulation results show that the performance of the system depends negligibly on the location of interference activity within the received word for a given value of ρ if the system employs code-symbol interleaving [4].

2.1.3 Receiver

The receiver is designed to detect the information originating at the transmitter that sends $s_0(t)$. The summand for $k = 0$ in (2.7) is thus the desired component in the received signal (or the *desired signal*, for short). For $1 \leq k \leq K-1$, the kth summand in (2.7) is the kth interference component in the received signal (the *kth interfering signal*). For example, if K=2, the received signal consists of the desired signal and one interfering signal. Substituting (2.6) into (2.7),

$$\begin{aligned} r(t) =& A_0\sqrt{2P_0}c_0^I(t)\cos(2\pi f_c t) + \sum_{k=1}^{K-1} A_k\sqrt{2P_k}c_k^I\left(\left(1+\frac{f_k}{f_c}\right)(t-\tau_k)\right)\cos(2\pi f_c t+\Phi_k)+ \\ & A_0\sqrt{2P_0}c_0^Q(t)\sin(2\pi f_c t) + \sum_{k=1}^{K-1} A_k\sqrt{2P_k}c_k^Q\left(\left(1+\frac{f_k}{f_c}\right)(t-\tau_k)\right)\sin(2\pi f_c t+\Phi_k)+ \\ & n(t) \end{aligned} \tag{2.8}$$

where $\Phi_k = \theta_k - 2\pi(f_c + f_k)\tau_k + 2\pi f_k t$ is the accumulated phase in the kth received signal component at time t=0. The receiver is illustrated in Figure 2.4. We consider a receiver that uses coherent demodulation and assume it achieves perfect symbol-timing synchronization with the desired signal and a local carrier reference with perfect phase and frequency synchronization with the desired signal. Without loss of generality, we assume that $\theta_0 = \tau_0 = f_0 = 0$ and we consider detection of information word $\underline{d}_0^{(0)}$.

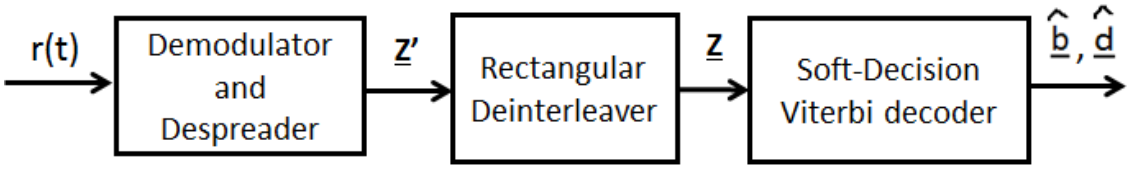

Figure 2.4: Receiver.

The signal received during the interval $[0, LT)$ is converted to the received word $\underline{Z}'$ by a demodulator and a despreader for $s_0(t)$. The received word is decoded to the detected information word $\underline{\hat{d}}$ using soft-decision Viterbi decoding. In Chapter 4 and afterwards in the thesis, we consider soft-decision Viterbi decoding using the correlator form of the optimal (maximum-likelihood sequence detection) path metric [5]. The received word is deinterleaved prior to decoding using a rectangular array in which the received symbols are written into the array by columns and read out of the array by rows. The deinterleaved received word is

$$\underline{Z} = (Z_0, ..., Z_{nL-1}). \tag{2.9}$$

2.1.4 Statistic for Each Binary Code Symbol

The output of the despreader is one statistic for each binary code symbol in the code word $\underline{b}_0^{(0)}$. The symbol statistic Z_i' corresponding to code symbol $b_{0,i}'$ is given by

$$\begin{aligned} Z_i' =& \int_{iT}^{(i+1)T} r(\tau) a_0^I(\tau) \cos(2\pi f_c \tau) d\tau + \int_{iT}^{(i+1)T} r(\tau) a_0^Q(\tau) \sin(2\pi f_c \tau) d\tau \\ =& S_{0,i} + \sum_{k=1}^{K-1} I_{k,i} + \eta_{0,i}. \end{aligned} \tag{2.10}$$

The term $S_{0,i}$ represents the contribution of the desired signal to the symbol statistic, and the term $I_{k,i}$ represents the contribution of multiple-access interference from the kth interfering signal. The term $\eta_{0,i}$ represents the contribution of the thermal noise to the decision statistic; it is a Gaussian random variable with mean zero and variance $\sigma_{\eta_{0,i}}^2 = \frac{N_0 T}{2}$. The deinterleaved statistics $\{Z_0, ..., Z_{nL-1}\}$ form the received word $\underline{Z}$ that is provided as input to the Viterbi decoder.

2.2 Measures of the Quality of the Received Signal

The signal-to-noise ratio, the signal-to-interference ratio and the signal-to-interference-plus-noise ratio of the desired signal at the receiver are used as the measures of the signal quality. The signal-to-noise ratio, γ_{SNR}, in the ith channel-symbol position is defined as the ratio of the (code-rate-normalized) desired-signal energy in Z_i to the mean noise energy in Z_i:

$$\gamma_{SNR} = \frac{L(E[Z_i]|b_{0,0})^2}{(L-m)\mathrm{Var}(\eta_{0,i}|b_{0,0})} \times \frac{1}{R_c}. \tag{2.11}$$

The signal-to-interference ratio, γ_{SIR}, in the ith channel-symbol position is defined as the ratio of the normalized desired-signal energy in Z_i to the mean interference energy in Z_i:

$$\gamma_{SIR} = \frac{L(E[Z_i]|b_{0,0})^2}{(L-m)\mathrm{Var}\left(\sum_{k=1}^{K-1} I_{k,i}|b_{0,0}\right)} \times \frac{1}{R_c}. \tag{2.12}$$

The signal-to-interference-plus-noise ratio, γ_{SINR}, in the ith channel-symbol position is defined as the ratio of the normalized desired-signal energy in Z_i to the sum of the mean noise energy and the mean interference energy in Z_i:

$$\gamma_{SINR} = \frac{L(E[Z_i]|b_{0,0})^2}{(L-m)\text{Var}\left(\left(\sum_{k=1}^{K-1} I_{k,i} + \eta_{0,i}\right)|b_{0,0}\right)} \times \frac{1}{R_c}. \tag{2.13}$$

2.3 Statistical Model of the Communication System

2.3.1 Transmitted Signal

The binary data symbols, $\{d_{k,i}\}$, $0 \le k \le K-1$, $0 \le i \le j(L-m)-1$ and the chip polarities, $\left\{a_{k,i}^I\right\}$ and $\left\{a_{k,i}^Q\right\}$, $0 \le k \le K-1$, $0 \le i \le nL-1$ are modeled as mutually independent Bernoulli random variables, with each random variable taking on the values 0 and 1, each with a probability of 1/2.

2.3.2 Received Signal

The time delays $\{\tau_k\}$ and the phase shifts $\{\Phi_k\}$, $1 \le k \le K-1$, are mutually independent random variables and they are mutually independent of the random variables discussed in Section (2.3.1). Several circumstances are considered in subsequent chapters. In one circumstance, the time delays and phase shifts are constant. In the other circumstances, either each time delay is uniformly distributed over [0,T], or each phase shift is uniformly distributed over [0,2π], or both. In all the circumstances, the parameters $\{P_k\}$, $\{A_k\}$, and $\{f_k\}$ are constant. In particular, we consider only $f_k = 0$ for all k in the following chapters.

Chapter 3

Characterization of the Receiver Statistics

In this chapter we characterize the code-symbol statistics at the receiver for the system introduced in Chapter 2 and develop a joint Gaussian approximation to their joint conditional distribution given the transmitted code word. The development is adapted from the analysis given in [3] for a DS-CDMA system with offset QPSK spread-spectrum data modulation in which the in-phase and quadrature spreading signals spread different (offset) binary data signals. The circumstance we consider thus differs from the circumstance considered in [3] in that the in-phase and quadrature spreading signals spread the same binary data signal with no time offset between the inphase and quadrature signals. The development in [3] addresses the effect of the Gaussian approximation on the probability of error in a channel-symbol decision at the output of the receiver's demodulator, whereas we use the Gaussian approximation in an approximation of the probability of code-word error at the output of the Viterbi decoder.

Without loss of generality, we consider the statistics Z_0' and Z_l' and develop closed-form expressions for their conditional first and second moments given the transmitted code word for each of four special cases. In the first case, the time delays and phase shifts of the interfering signals are constant. In the second case, each carrier's phase shift at the

receiver for each interfering signal is uniformly distributed over [0,2π] but their time delays are constant. In the third case, the time delay at the receiver for each interfering signal is uniformly distributed over [0,T] but its phase shift is constant. In the fourth case, each time delay is uniformly distributed over [0,T] and each phase shift is uniformly distributed over [0,2π].

In all that follows, conditioning on $b'_{0,0}$ is implicit. Following [3], from equation (2.9),

$$E[S_{0,0}] = (-1)^{b'_{0,0}} T A_0 \sqrt{2P_0} \tag{3.1}$$

and

$$\mathrm{Var}(\eta_{0,0}) = \frac{N_0 T}{2}. \tag{3.2}$$

Furthermore,

$$I_{k,0} = \sqrt{\frac{A_k^2 P_k}{2}} \left(W_k^I + W_k^Q \right) \tag{3.3}$$

where

$$W_k^I = U_k^I \cos(\Phi_k) + V_k^I \sin(\Phi_k) \tag{3.4}$$

$$W_k^Q = U_k^Q \cos(\Phi_k) - V_k^Q \sin(\Phi_k) \tag{3.5}$$

$$U_k^I = \left(\int_0^T A_k \sqrt{2P_k} c_k^I (\tau - \tau_k) \cos(2\pi f_c \tau + \Phi_k) a_0^I(\tau) \cos(2\pi f_c \tau) d\tau \right) \Big/ \cos(\Phi_k) \tag{3.6}$$

$$U_k^Q = \left(\int_0^T A_k \sqrt{2P_k} c_k^Q (\tau - \tau_k) \sin(2\pi f_c \tau + \Phi_k) a_0^Q(\tau) \sin(2\pi f_c \tau) d\tau \right) \Big/ \cos(\Phi_k) \tag{3.7}$$

$$V_k^I = \left(\int_0^T A_k \sqrt{2P_k} c_k^Q (\tau - \tau_k) \sin(2\pi f_c \tau + \Phi_k) a_0^I(\tau) \cos(2\pi f_c \tau) d\tau \right) \Big/ \sin(\Phi_k) \tag{3.8}$$

$$V_k^Q = \left(\int_0^T A_k \sqrt{2P_k} c_k^I (\tau - \tau_k) \cos(2\pi f_c \tau + \Phi_k) a_0^Q(\tau) \sin(2\pi f_c \tau) d\tau \right) \Big/ \sin(\Phi_k). \tag{3.9}$$

The random variables $\{U_k^I, U_k^Q, V_k^I, V_k^Q\}$, $1 \leq k \leq K-1$, can be expressed in terms of random variables involving discrete cross-correlation functions of the spreading sequences and the chip-pulse continuous partial autocorrelation functions [3]. For example, the random variable U_k^I can be expressed as

$$\begin{aligned} U_k^I = & \sum_{i=0}^{N-2} H_{k,i}^I [\hat{R}_{\psi_c}(S_k) + a_{0,i}^I a_{0,i+1}^I R_{\psi_c}(S_k)] \\ & + H_{k,N-1}^I \hat{R}_{\psi_c}(S_k) + H_{k,N}^I R_{\psi_c}(S_k) \end{aligned} \tag{3.10}$$

where

$$H_{k,i}^I = \begin{cases} (-1)^{b'_{k,-1}} a_{k,i-\gamma_k}^I a_{0,i}^I, & \text{if } 0 \leq i \leq \gamma_k - 1 \\ (-1)^{b'_{k,0}} a_{k,i-\gamma_k}^I a_{0,i}^I, & \text{if } \gamma_k \leq i \leq N-1 \\ (-1)^{b'_{k,-1}} a_{k,-\gamma_k-1}^I a_{0,0}^I, & \text{if } i = N \end{cases} . \tag{3.11}$$

The chip delay random variable S_k is given by $S_k = \tau_k - \gamma_k T_c$, with $\gamma_k = \lfloor \tau_k / T_c \rfloor$. The chip autocorrelation functions are given by

$$R_{\psi_c}(s) = \int_0^s \psi_c(t) \psi_c(t + T_c - s) dt \tag{3.12}$$

and

$$\hat{R}_{\psi_c}(s) = \int_s^{T_c} \psi_c(t) \psi_c(t - s) dt. \tag{3.13}$$

Similarly, the random variable U_k^Q can be expressed as

$$\begin{aligned} U_k^Q = &\sum_{i=0}^{N-2} H_{k,i}^Q [\hat{R}_{\psi_c}(S_k) + a_{0,i}^Q a_{0,i+1}^Q R_{\psi_c}(S_k)] \\ &+ H_{k,N-1}^Q \hat{R}_{\psi_c}(S_k) + H_{k,N}^Q R_{\psi_c}(S_k) \end{aligned} \tag{3.14}$$

where

$$H_{k,i}^Q = \begin{cases} (-1)^{b'_{k,-1}} a_{k,i-\gamma_k}^Q a_{0,i}^Q, & \text{if } 0 \le i \le \gamma_k - 1 \\ (-1)^{b'_{k,-0}} a_{k,i-\gamma_k}^Q a_{0,i}^Q, & \text{if } \gamma_k \le i \le N-1 \\ (-1)^{b'_{k,-1}} a_{k,-\gamma_k-1}^Q a_{0,0}^Q, & \text{if } i = N \end{cases} . \tag{3.15}$$

The random variable V_k^I can be expressed as

$$\begin{aligned} V_k^I = &\sum_{i=0}^{N-2} \tilde{H}_{k,i}^I [\hat{R}_{\psi_c}(S_k) + a_{0,i}^I a_{0,i+1}^I R_{\psi_c}(S_k)] \\ &+ \tilde{H}_{k,N-1}^I \hat{R}_{\psi_c}(S_k) + \tilde{H}_{k,N}^I R_{\psi_c}(S_k) \end{aligned} \tag{3.16}$$

where

$$\tilde{H}_{k,i}^I = \begin{cases} (-1)^{b'_{k,-1}} a_{k,i-\gamma_k}^Q a_{0,i}^I, & \text{if } 0 \le i \le \gamma_k - 1 \\ (-1)^{b'_{k,-0}} a_{k,i-\gamma_k}^Q a_{0,i}^I, & \text{if } \gamma_k \le i \le N-1 \\ (-1)^{b'_{k,-1}} a_{k,-\gamma_k-1}^Q a_{0,0}^I, & \text{if } i = N \end{cases} . \tag{3.17}$$

And the random variable V_k^Q can be expressed as

$$\begin{aligned} V_k^Q = &\sum_{i=0}^{N-2} \tilde{H}_{k,i}^Q [\hat{R}_{\psi_c}(S_k) + a_{0,i}^Q a_{0,i+1}^Q R_{\psi_c}(S_k)] \\ &+ \tilde{H}_{k,N-1}^Q \hat{R}_{\psi_c}(S_k) + \tilde{H}_{k,N}^Q R_{\psi_c}(S_k) \end{aligned} \tag{3.18}$$

where

$$\tilde{H}_{k,i}^Q = \begin{cases} (-1)^{b'_{k,-1}} a_{k,i-\gamma_k}^I a_{0,i}^Q, & \text{if } 0 \le i \le \gamma_k - 1 \\ (-1)^{b'_{k,0}} a_{k,i-\gamma_k}^I a_{0,i}^Q, & \text{if } \gamma_k \le i \le N-1 \\ (-1)^{b'_{k,-1}} a_{k,-\gamma_k-1}^I a_{0,0}^Q, & \text{if } i = N \end{cases} . \tag{3.19}$$

Under the independence conditions of Section 2.3, the random variables $\{H_{k,i}^I,\ H_{k,i}^Q,\ \tilde{H}_{k,i}^I,\ \tilde{H}_{k,i}^Q\}$, $1 \le k \le K-1$, $0 \le i \le N$, are mutually independent and identically distributed (i.i.d.) equally likely Bernoulli random variables, as can be shown following an argument in [6]. Define the correlation parameters

$$C \triangleq \sum_{i=0}^{N-2} a_{0,i}^Q a_{0,i+1}^Q, 1 \le k \le K-1, \tag{3.20}$$

and

$$D \triangleq \sum_{i=0}^{N-2} a_{0,i}^I a_{0,i+1}^I, 1 \le k \le K-1. \tag{3.21}$$

The random variables $\{U_k^I, U_k^Q, V_k^I, V_k^Q\}$, $1 \le k \le K-1$, are conditionally mutually independent given $\{C, D, \{\Phi_k, \tau_k\}, 1 \le k \le K-1\}$, again following an argument in [6]. Thus, the conditional covariances of any two of the random variables is zero. Similarly, $\{W_k^I, W_k^Q\}$, $1 \le k \le K-1$, are conditionally mutually independent given $\{C, D, \{\Phi_k, \tau_k\}, 1 \le k \le K-1\}$.

Now let us consider the first moment and variance of each of the random variables. It is helpful to decompose the expression for each into useful auxiliary random variables. As an example, we will consider the case of U_k^Q. Define the disjoint sets of indices

$$A \triangleq \{i, 0 \le i \le N-2, \text{ such that } a_{0,i}^Q a_{0,i+1}^Q = 1\} \tag{3.22}$$

and

$$B \triangleq \{i, 0 \le i \le N-2, \text{ such that } a_{0,i}^Q a_{0,i+1}^Q = -1\}. \tag{3.23}$$

Then

$$U_k^Q = \lambda_k \hat{R}_{\psi_c}(S_k) + \mu_k R_{\psi_c}(S_k) \tag{3.24}$$

where the discrete random variables λ_k and μ_k are given by

$$\lambda_k = X_k + Y_k + H_{k,N-1} \tag{3.25}$$

$$\mu_k = X_k - Y_k + H_{k,N} \tag{3.26}$$

and the discrete variables X_k and Y_k are defined by

$$X_k \triangleq \sum_{i \epsilon A} H_{k,i} \tag{3.27}$$

and

$$Y_k \triangleq \sum_{i \epsilon B} H_{k,i}. \tag{3.28}$$

The random variables $\{\lambda_k, \mu_k, \Phi_k, \tau_k\}, 1 \leq k \leq K-1$, are conditionally mutually independent given C and $\{\Phi_k, \tau_k\}$, $1 \leq k \leq K-1$, is independent of C.

It follows that

$$E[\lambda_k] = E[\mu_k] = E[\lambda_k \mu_k] = 0 \tag{3.29}$$

and, using equation (3.24) and the independence conditions of Section 2.3, we have

$$\begin{aligned} E[U_k^Q] &= E[\lambda_k \hat{R}_{\psi_c}(S_k) + \mu_k R_{\psi_c}(S_k)] \\ &= E[\hat{R}_{\psi_c}(S_k)]E[\lambda_k] + E[R_{\psi_c}(S_k)]E[\mu_k] = 0. \end{aligned} \tag{3.30}$$

In a similar manner,

$$E[V_k^Q] = E[U_k^I] = E[V_k^I] = 0. \tag{3.31}$$

Therefore,

$$\begin{aligned} E[I_{k,0}] &= E\left[\sqrt{\frac{A_k^2 P_k}{2}}\left(U_k^I\cos(\Phi_k) + V_k^I\sin(\Phi_k) + U_k^Q\cos(\Phi_k) - V_k^Q\sin(\Phi_k)\right)\right] \\ &= \sqrt{\frac{A_k^2 P_k}{2}}\left(E[U_k^I]E[\cos(\Phi_k)] + E[V_k^I]E[\sin(\Phi_k)]\right. \\ &\qquad \left. + E[U_k^Q]E[\cos(\Phi_k)] - E[V_k^Q]E[\sin(\Phi_k)]\right) \\ &= 0 \end{aligned} \tag{3.32}$$

from equations (3.30) and (3.31) and the independence conditions of Section 2.3.

Now we will proceed to find the expression for the variance of the multiple-access interference term in equation (2.10). From the independence conditions of Section 2.3,

$$\mathrm{Var}\left(\sum_{k=1}^{K-1} I_{k,0}\right) = \sum_{k=1}^{K-1} \mathrm{Var}\left(I_{k,0}\right). \tag{3.33}$$

And from the same independence conditions and equations (3.30) and (3.31),

$$\begin{aligned} \mathrm{Var}\left(I_{k,0}\right) =& \frac{1}{2}\mathrm{Var}\left[\sqrt{A_k^2 P_k}(W_k^I + W_k^Q)\right] \\ =& \frac{1}{2}A_k^2 P_k\Big(E[(U_k^I)^2]E[\cos^2(\Phi_k)] + E[(V_k^I)^2]E[\sin^2(\Phi_k)] \\ &+ E[(U_k^Q)^2]E[\cos^2(\Phi_k)] + E[(V_k^Q)^2]E[\sin^2(\Phi_k)]\Big). \end{aligned} \tag{3.34}$$

Furthermore,

$$\begin{aligned} E[(U_k^Q)^2] =& E[(\lambda_k \hat{R}_{\psi_c}(S_k) + \mu_k R_{\psi_c}(S_k))^2] \\ =& E[\lambda_k^2]E[(\hat{R}_{\psi_c}(S_k))^2] + E[\mu_k^2]E[(R_{\psi_c}(S_k))^2] \end{aligned} \tag{3.35}$$

from equation (3.24) and the independence conditions of Section 2.3. Similar expressions result for $E[(U_k^I)^2], E[(V_k^I)^2]$, and $E[(V_k^Q)^2]$. Finally,

$$E[\lambda_k^2] = E[\mu_k^2] = N. \tag{3.36}$$

Thus,

$$\begin{aligned}\mathrm{Var}\,(I_{k,0}) =&\frac{1}{2}A_k^2P_k\Big(2(NE[(R_{\psi_c}(S_k))^2]+NE[(\hat{R}_{\psi_c}(S_k))^2])E[\cos^2(\Phi_k)]\\ &+2(NE[(R_{\psi_c}(S_k))^2]+NE[(\hat{R}_{\psi_c}(S_k))^2])E[\sin^2(\Phi_k)]\Big)\\ =&A_k^2P_kN\Big((E[(R_{\psi_c}(S_k))^2]+E[(\hat{R}_{\psi_c}(S_k))^2])(E[\cos^2(\Phi_k)]+E[\sin^2(\Phi_k)])\Big)\\ =&A_k^2P_kN\Big(E[(R_{\psi_c}(S_k))^2]+E[(\hat{R}_{\psi_c}(S_k))^2]\Big).\end{aligned} \tag{3.37}$$

Note that equation (3.37) does not depend on the distribution function of Φ_k.

Case 1: Consider the case where $\{\Phi_k, \tau_k\}$, $1 \le k \le K-1$ are constant. Let $S_k = s_k$, where s_k is a constant.

We consider the rectangular chip pulse waveform, for which the partial autocorrelation functions are given by

$$R_{\psi_c}(s) = s \tag{3.38}$$

and

$$\hat{R}_{\psi_c}(s) = T_c - s. \tag{3.39}$$

From equation (3.37),

$$\mathrm{Var}\,(I_{k,0}) = A_k^2P_kN(T_c^2 + 2s_k^2 - 2T_cs_k). \tag{3.40}$$

Case 2: The analysis of case 1 applies, so the variance of $I_{k,0}$ is given by equation (3.40).

Case 3: Consider the case where τ_k is uniformly distributed over [0,T] but Φ_k is constant.

$$E[(R_{\psi_c}(S_k))^2] + E[(\hat{R}_{\psi_c}(S_k))^2] = \frac{2}{T_c}\int_0^{T_c} R_{\psi_c}^2(s)ds = 2T_c^2M_c \tag{3.41}$$

where the term $M_c \triangleq \frac{1}{T_c^3}\int_0^{T_c} R_{\psi_c}^2(s)ds$ represents a chip mean-squared correlation parameter that depends on the actual shape of the chip waveform $\psi_c(t)$. We consider the rectangular chip pulse waveform, for which the partial autocorrelation functions are given by equations

(3.38) and (3.39). Thus, $M_c = 1/3$, and

$$E[(R_{\psi_c}(S_k))^2] + E[(\hat{R}_{\psi_c}(S_k))^2] = \frac{2}{3}T_c^2. \tag{3.42}$$

From equation (3.37),

$$\text{Var}\,(I_{k,0}) = \frac{2}{3}A_k^2 P_k N T_c^2. \tag{3.43}$$

Case 4: The analysis of Case 3 applies, so the variance of $I_{k,0}$ is given by (3.43). For cases 1 and 2, the signal-to-interference-plus-noise ratio in channel-symbol position zero is given by

$$\begin{aligned}\gamma_{SINR} &= \frac{2L(E[Z_0'])^2}{(L-m)\text{Var}\left(\sum_{k=1}^{K-1} I_{k,0} + \eta_{0,0}\right)} \\ &= \frac{4LA_0^2P_0T^2}{(L-m)(\frac{N_0T}{2} + \sum_{k=1}^{K-1} A_k^2P_kN(T_c^2 + 2s_k^2 - 2T_cs_k))} \\ &= \frac{8LA_0^2P_0T^2}{(L-m)(N_0T + 2\sum_{k=1}^{K-1} A_k^2P_kN(T_c^2 + 2s_k^2 - 2T_cs_k))}.\end{aligned} \tag{3.44}$$

For cases 3 and 4, it is given by

$$\begin{aligned}\gamma_{SINR} &= \frac{2L(E[Z_0'])^2}{(L-m)\text{Var}\left(\sum_{k=1}^{K-1} I_{k,0} + \eta_{0,0}\right)} \\ &= \frac{8LA_0^2P_0T}{(L-m)(N_0 + 4\sum_{k=1}^{K-1} A_k^2P_kT/3N)}.\end{aligned} \tag{3.45}$$

In a similar manner to the development above, it can be shown that the same results hold for each Z_l' for which interference is present in the corresponding symbol interval and analogous results hold with K=1 for each Z_l' for which interference is absent. Regardless, it is shown in a similar manner that Z_{l_1}' and Z_{l_2}' are conditionally uncorrelated given b_{0,l_1}' and b_{0,l_2}' for $l_1 \neq l_2$.

In the subsequent chapters, we compare the performance of two systems. The first system is the DS-CDMA system defined in Chapter 2, in which the desired signal is

subjected to both thermal noise and multiple-access interference at the receiver. In the second system, the effect of the interference on the receiver statistics is approximated by replacing each interference term $I_{k,l}$ with a zero-mean Gaussian random variable $\tilde{I}_{k,l}$ such that the $\mathrm{Var}(\tilde{I}_{k,l})$=$\mathrm{Var}(I_{k,l})$. The random variables $\{I_{k,l}, \eta_{k,l}\}$, $1 \leq k \leq K-1$, $0 \leq l \leq nL-1$ are independent. The second system thus approximates the first system using the SGA. Two bounds on the probability of code-word error are considered in Chapter 5, and both use the SGA (i.e., the model of the second system).

Chapter 4

Effect of the SGA on Pairwise Error-Event Probabilities

In this chapter, we gain insight into the effect of the SGA on the probability of error at the output of the soft-decision Viterbi decoder by considering the pairwise error-event probability [4] in the decoder for error events of different Hamming weights. The interference activity ρ=1. The receiver of the soft-decision Viterbi decoder provides maximum-likelihood detection of the code word based on the continuous-valued channel outputs. We assume without loss of generality that the all-zeros sequence is the actual transmitted sequence.

Let $\underline{Z} = (Z_0, .., Z_{nL-1})$ denote the deinterleaved channel outputs under the condition that the code sequence $\underline{b}_0^{(0)} = (b_0, .., b_{nL-1}) = \underline{0}$. Suppose $\underline{b}_q^{q+l-1} = (b_q, ..., b_{q+l-1})$ is a length-l subsequence of $\underline{b}_0^{(0)}$ and $\underline{\tilde{b}}_q^{q+l-1} = (\tilde{b_q}, ..., \tilde{b}_{q+l-1})$ is the corresponding subsequence of code sequence $\underline{\tilde{b}}$ for which the encoder states agree at times q and $q+l$ in the generation of the two sequences. Suppose d is the Hamming distance between the two code subsequences and that they differ in code-symbol positions $i_0, ..., i_{d-1}$. That is $\tilde{b}_{i_j} = 1$, $0 \leq j \leq d-1$, and $\tilde{b}_{i_j} = 0$ for all i, $q \leq i \leq q+l-1$, such that $i \notin \{i_o, .., i_{d-1}\}$.

Among the two subsequences, the soft-decision Viterbi decoder will prefer the subsequence with the larger correlator-form path metric [5]. The path metric for $\underline{b}_q^{q+l-1}$ is given

by

$$M = \sum_{i=q}^{q+l-1} Z_i(-1)^{b_i} = \sum_{i=q}^{q+l-1} Z_i, \tag{4.1}$$

and the path metric for $\underline{\tilde{b}}_q^{q+l-1}$ is given by

$$\begin{aligned} \tilde{M} &= \sum_{i=q}^{q+l-1} Z_i(-1)^{\tilde{b_i}} \\ &= \sum_{i=q \text{ s.t. } \tilde{b_i}=0}^{q+l-1} Z_i - \sum_{i=q \text{ s.t.} \tilde{b_i}=1}^{q+l-1} Z_i. \end{aligned} \tag{4.2}$$

The probability of the pairwise error-event $\{\tilde{M} > M\}$ is thus given by

$$\begin{aligned} P(\tilde{M} > M) &= P\left(- \sum_{i=q \text{ s.t. } \tilde{b_i}=1}^{q+l-1} Z_i > \sum_{i=q \text{ s.t. } \tilde{b_i}=1}^{q+l-1} Z_i \right) \\ &= P\left(\sum_{i=q \text{ s.t. } \tilde{b_i}=1}^{q+l-1} Z_i < 0 \right) \\ &= P(X < 0) \end{aligned} \tag{4.3}$$

where

$$X = \sum_{j=0}^{d-1} Z_{i_j}. \tag{4.4}$$

Suppose the SGA is used to approximate the effect of the multiple-access interference on the receiver statistics of the system in Chapter 2 with soft-decision Viterbi decoding. Then $\{Z_{i_0}, ..., Z_{i_{l-1}}\}$ are independent, identically distributed Gaussian random variables with

$$E[Z_{i_j}] = TA_0\sqrt{2P_0} \tag{4.5}$$

from equation (2.10) and

$$\text{Var}(Z_{i_j}) = \frac{N_0 T}{2} + \sum_{k=1}^{K-1} A_k^2 P_k N \left(E[(R_{\psi_c}(S_k))^2] + E[(\hat{R}_{\psi_c}(S_k))^2] \right) \tag{4.6}$$

from equations (3.2) and (3.37). (The form of the latter equation can be simplified in any of the four cases considered in the previous chapter.) Then

$$\begin{aligned} P(\tilde{M} > M) =& Q\left(\frac{dE[Z_{i_0}]}{\sqrt{d\mathrm{Var}(Z_{i_0})}}\right) \\ =& Q\left(\sqrt{\frac{2dA_0^2P_0T^2}{(\frac{N_0T}{2} + \sum_{k=1}^{K-1} A_k^2P_kN(E[(R_{\psi_c}(S_k))^2] + E[(\hat{R}_{\psi_c}(S_k))^2]))}}\right) \\ =& Q\left(\sqrt{\frac{2dE_c}{(N_0 + \sum_{k=1}^{K-1} 2A_k^2P_kN(E[(R_{\psi_c}(S_k))^2] + E[(\hat{R}_{\psi_c}(S_k))^2]))}}\right) \end{aligned} \tag{4.7}$$

where E_c is the energy per channel symbol at the receiver. For example, if $\Phi_k = \tau_k = 0$ for $1 \le k \le K-1$ and all the signals are received with the same strength,

$$P(\tilde{M} > M) = Q\left(\sqrt{\frac{2dE_c}{(N_0 + (K-1)E_c/N)}}\right). \tag{4.8}$$

Thus in two limiting cases,

$$P(\tilde{M} > M) = Q\left(\sqrt{\frac{2dE_c}{N_0}}\right) \tag{4.9}$$

if no multiple-access interference is present in the received signal, and

$$P(\tilde{M} > M) = Q\left(\sqrt{\frac{2dN}{K-1}}\right) \tag{4.10}$$

if no thermal noise is present in the received signal.

The effect of the SGA on the accuracy of the pairwise error-event probability is illustrated by considering the system of Chapter 2 using soft-decision Viterbi decoding with a spreading factor of 31 chips per binary channel symbol ($N = 31$), a single interfering signal ($K = 2$) that is chip synchronous and phase synchronous with the desired signal, and interference activity ρ=1. The desired signal and the interfering signal arrive at the receiver with the same power.

The pairwise error-event probability in the decoder is illustrated in Figure 4.1 for

several values of the Hamming distance of the error event. The solid lines in the figure show pairwise error-event probabilities for the system with the single interference, and the dashed lines show corresponding probabilities for a system in which the interference has been replaced by equivalent Gaussian noise using the SGA. The probabilities obtained with the SGA are given by equation (4.8). For each value of the Hamming distance and each value of the signal-to-noise ratio at the receiver, the approximation to the pairwise error-event probability based on the SGA is greater than the probability for the system with multiple-access interference. For small values of the Hamming distance (e.g., $d = 1$ and $d = 2$), the approximation using the SGA is poorer than the actual pairwise error-event probability for probabilities greater than 10^{-3}. For a given pairwise error-event probability, however, the accuracy of the approximation improves as the Hamming distance of the error event increases. For error events of Hamming weight 5 or greater, the approximation and the actual error probability are in close agreement if the pairwise error-event probability is 10^{-5} or greater. (For error events of Hamming weight 6 or greater, the difference is indiscernible in the figure.) The results suggest that the SGA yields an accurate approximation to performance of this system if the convolutional code has a minimum Hamming distance of at least six - a hypothesis investigated in Chapter 6.

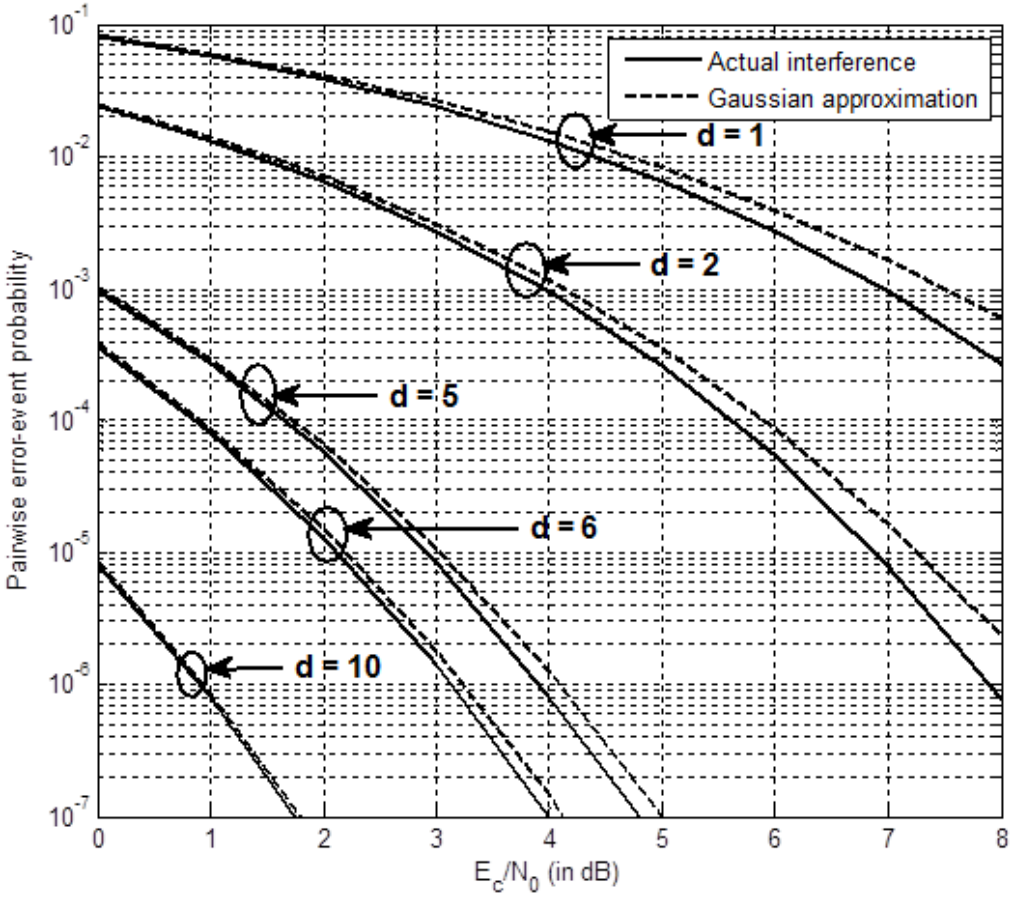

Figure 4.1: Pairwise error-event probability as a function of Hamming distance.

Chapter 5

Bounds on the Probability of Code-Word Error with Soft-Decision Viterbi Decoding

In this chapter, we describe two previously developed bounds on the probability of code-word error for soft-decision Vitberi decoding: the *concave-first-event bound* and the *concave-integral bound*. Both provide an upper bound on the probability of code-word error at the output of the decoder for the system described in Chapter 2 using soft-decision Viterbi decoding if the received signal is subjected to time-varying additive white Gaussian noise and code-symbol interleaving. Both are used in the next chapter in conjunction with the SGA to provide a closed-form approximation to the probability of code-word error if the system is also subjected to multiple-access interference.

The bounds are developed in [4] utilizing results presented in [7] and [8]. A comparison is presented in [4] between the bounds and the probability of code-word error for a system using convolutional coding and binary antipodal modulation. Here we extend their use to the communication system described in Chapter 2 in which quaternary, direct-sequence spread-spectrum modulation is used.

5.1 Concave-First-Event Bound

The probability of code-word error is represented by P_e. The concave-first-event bound is expressed as

$$P_e \leq 1 - (1-p)^L \tag{5.1}$$

where p is the first-event error probability [7] at time 0 for a transmission of block length L [4]. The first-event error probability is obtained through simulation for the specified system and each channel of interest.

5.2 Concave-Integral Bound

The first-event union bound [4] is expressed as

$$P_u = \frac{1}{\pi} \int_0^{\frac{\pi}{2}} T(W)|_{W=(1-\rho)\exp(-\frac{E_c}{N_0})+\rho\exp(-\frac{E_c}{N_1})} d\theta \tag{5.2}$$

where T(W) is the path enumerator of the binary convolutional code [5] and the interference activity is ρ. The parameter N_0 represents the noise power spectral density when interference is absent and the parameter N_1 represents the equivalent noise plus interference power spectral density when interference is present. The integral form of the concave bound [4] is expressed as

$$P_e \leq 1 - (1-P_u)^L \tag{5.3}$$

where P_u is as expressed in (5.2).

Chapter 6

Approximation of the Performance Using the SGA and Bounds

In this chapter we consider the system in Chapter 2 using soft-decision Viterbi decoding and its probability of code-word error in the presence of multiple-access interference. We compare its performance (which is obtained by Monte Carlo simulation) with three approximations to the performance. In the first approximation, the effect of the multiple-access interference on each receiver statistic is approximated by a Gaussian interference term (i.e., the SGA is used) and the performance of the approximating system is evaluated by simulation. The second approximation is obtained by applying the concave-first-event bound of Chapter 5 to the system with the SGA. The first-event error probability required for the bound is obtained by Monte Carlo simulation of the system with the SGA. The third approximation is obtained by applying the concave-integral bound of Chapter 5 to the system with the SGA.

As examples in this chapter, we consider systems using three rate-1/2 convolutional encoders: the memory-order-two encoder with $\mathbf{G} = (7,\ 5)$ (octal representation [5]) and $d_{min} = 5$, the memory-order-three encoder with $\mathbf{G} = (13,\ 15)$ and $d_{min} = 6$, and the memory-order-six CCSDS (NASA standard) encoder [9] with $\mathbf{G} = (171,\ 133)$ and $d_{min} = 10$. The information block-length L is 1000 information bits and tail bits so that each code word

contains 2000 binary code symbols. Each system uses a 50×40 rectangular interleaver at the transmitter and a 50×40 rectangular deinterleaver at the receiver. The concave-integral bound requires the path enumerator for the convolutional code under consideration. The path enumerators for the memory-order-two and memory-order-three codes are determined easily using Mason's theorem [5], and the path enumerator T(W) for the rate-1/2, NASA standard code is given in [10].

6.1 Accuracy of the Approximations

The accuracy of each approximation to the probability of code-word error is examined in this section by considering examples with the three convolutional codes noted above and three values of the interference activity: $\rho = 0$, $\rho = 0.5$, and $\rho = 1$. A single interfering signal is considered that is chip synchronous and phase synchronous with the desired signal. (Thus, $K = 2$.) There are 31 quaternary chips per binary channel symbol so that $N = 31$. The interfering signal arrives at the signal with the same power as the desired signal. In each example, the performance of the actual system and the performance of the system using the SGA are so close that the graphs are indiscernible on the scale used in the figures. Consequently, the graph for the simulated system using the SGA is not included in any of the figures.

The performance of the system with an encoder of memory order of two is shown in Figures 6.1, 6.2, and 6.3 for different values of ρ. The performance of the memory-order-two system with no interference (i.e. $\rho = 0$) is shown in Figure 6.1. The concave-first-event bound closely matches the actual probability of code-word error. It is accurate to within 0.1 dB if the probability of code-word error is 10^{-3} or greater. The concave-integral bound is looser than the concave-first-event bound. It differs from the actual probability of error by as much as 1.5 dB for some values of the probability of error greater than 10^{-3} and by 0.6 dB if $P_e = 10^{-3}$.

The probability of code-word error of the memory-order-two system with an inter-

ference activity of one-half ($\rho = 0.5$) is shown in Figure 6.2. The concave-first-event bound again closely matches the actual probability of code-word error obtained by simulation. The difference is within 0.2 dB if the probability of code-word error is 10^{-3} or greater. The concave-integral bound once again differs from the actual probability of error by as much as 1.5 dB if $P_e \geq 10^{-3}$ and by 0.55 dB if $P_e = 10^{-3}$.

Figure 6.3 illustrates the performance and the bounds for the memory-order-two system if interference is present throughout the transmission (i.e., $\rho = 1$). The concave-first-event bound again provides a close estimate of the actual probability of code-word error. The difference is within 0.35 dB if the probability of code-word error is 10^{-3} or greater. The concave-integral bound once again differs from the actual probability of error by as much as 1.5 dB if $P_e \geq 10^{-3}$ and by 0.5 dB if $P_e = 10^{-3}$. Thus it is seen that the concave-first-event bound provides a very accurate approximation of the performance of the memory-order-two system regardless of the interference activity of the channel. The accuracy of concave-integral bound is poorer than the concave-first-event bound. However, its accuracy improves as the probability of error decreases.

The performance of the system with an encoder of memory order of three is shown in Figures 6.4, 6.5, and 6.6 for different values of ρ. The performance of the memory-order-three system with no interference is shown in Figure 6.4. The concave-first-event bound closely matches the actual probability of code-word error. It is accurate to within 0.1 dB if the probability of code-word error is 10^{-3} or greater. The concave-integral bound differs from the actual probability of error by as much as 1.5 dB for some values of the probability of error greater than 10^{-3} and by 0.6 dB if $P_e = 10^{-3}$.

The probability of code-word error of the memory-order-three system with an interference activity of one-half is shown in Figure 6.5. The concave-first-event bound again closely matches the actual probability of code-word error obtained by simulation, though they differ by as much as 0.2 dB for some values of the probability of code-word error greater than 10^{-3}. The concave-integral bound once again differs from the actual probability of error by as much as 1.5 dB if $P_e \geq 10^{-3}$ and by 0.55 dB if $P_e = 10^{-3}$.

Figure 6.6 illustrates the performance and the bounds for the memory-order-three system if interference is present throughout the transmission. The concave-first-event bound again provides a close estimate of the actual probability of code-word error. It is accurate to within 0.35 dB if the probability of code-word error is 10^{-3} or greater. The concave-integral bound once again differs from the actual probability of error by as much as 1.5 dB if $P_e \geq 10^{-3}$ and by 0.5 dB if $P_e = 10^{-3}$. The relationship between either bound and the actual probability of error is similar to that observed with the system of memory order two.

The performance of the system with the NASA-standard encoder (with a memory order of six) is shown in Figures 6.7, 6.8, and 6.9 for different values of ρ. The performance of the memory-order-six system with no interference is shown in Figure 6.7. The concave-first-event bound closely matches the actual probability of code-word error. It is accurate to within 0.2 dB if the probability of code-word error is 10^{-3} or greater. The concave-integral bound differs from the actual probability of error by as much as 1.5 dB for some values of the probability of error greater than 10^{-3}, the difference is 0.65 dB if $P_e = 10^{-2}$, and it is 0.55 dB if $P_e = 10^{-3}$.

The probability of code-word error of the memory-order-six system with an interference activity of one-half is shown in Figure 6.8. The concave-first-event bound again closely matches the actual probability of code-word error obtained by simulation, differing by 0.35 dB or less if the probability of code-word error is greater than 10^{-3}. The concave-integral bound differs from the actual probability of error by as much as 1.5 dB for some values of the probability of error greater than 10^{-3}, but it differs from the actual probability of error by only 0.55 dB if $P_e = 10^{-2}$ and by 0.5 dB if $P_e = 10^{-3}$.

Figure 6.9 illustrates the performance and the bounds for the memory-order-six system if interference is present throughout the transmission. The concave-first-event bound again provides a close estimate of the actual probability of code-word error. It is accurate to within 0.5 dB if the probability of code-word error is 10^{-3} or greater. The concave-integral bound once again differs from the actual probability of error by as much as 1.5 dB if $P_e \geq 10^{-3}$ but the difference is only 0.4 dB if $P_e = 10^{-2}$ and 0.25 dB if $P_e = 10^{-3}$.

The relationship between either bound and the actual probability of error is similar to that observed with the systems of memory orders two and three.

In all of the examples, the concave-first-event bound closely matches the actual probability of code-word error obtained by simulation. The concave-integral bound provides a looser bound on the probability of code-word error: in all the cases, the concave-first-event bound is strictly tighter than the concave-integral bound. Both bounds are more accurate if the channel is good than if it is bad; that is, their tightness increases as the probability of code-word error is decreased.

In other respects, the two bounds behave in a contrary manner. The tightness of the concave-integral bound improves as the interference activity, ρ, increases, however, whereas the tightness of the concave-first-event bound declines slightly as ρ increases. Similarly, the concave-first-event bound is slightly less accurate with a better code than with a weaker code, whereas the accuracy of the concave-integral bound improves noticeably as the memory order (and minimum Hamming distance) of the code is increased.

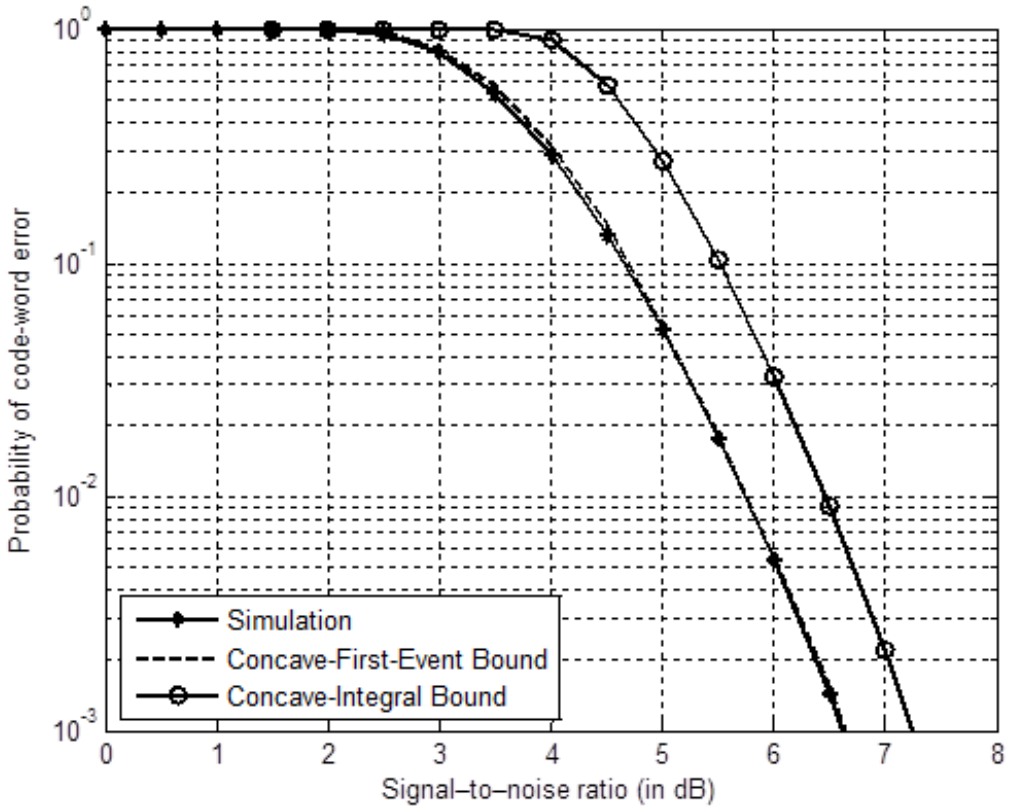

Figure 6.1: Comparison of bounds for memory-order-two encoder (ρ=0).

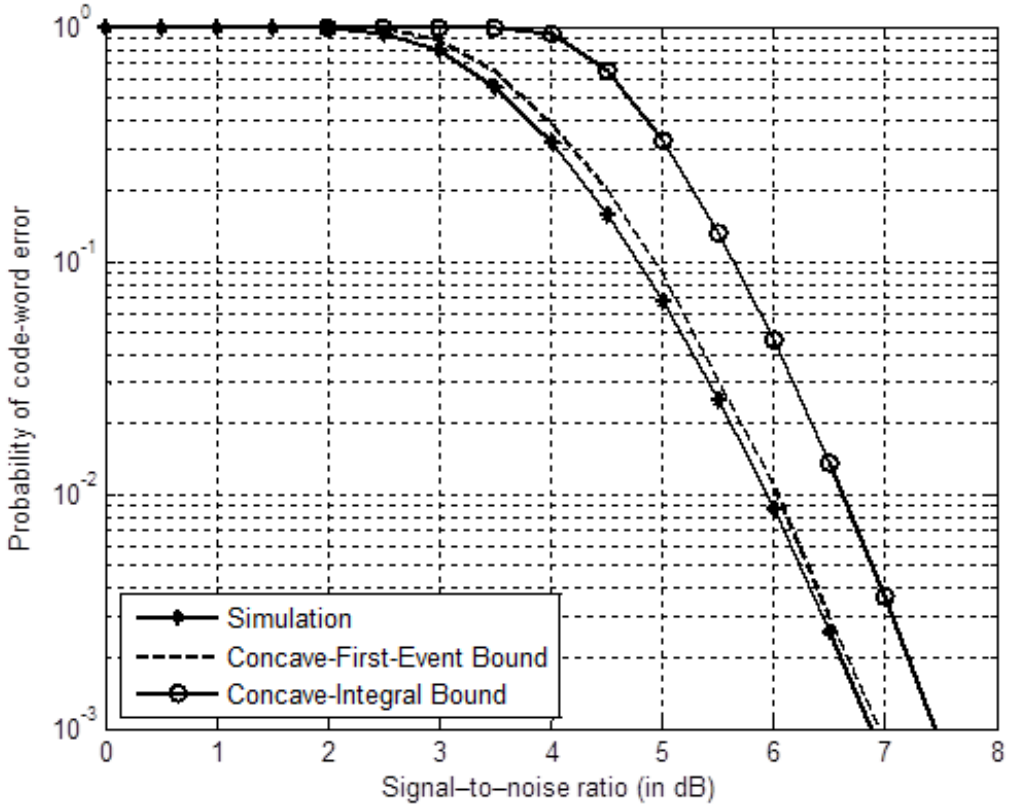

Figure 6.2: Comparison of bounds for memory-order-two encoder (ρ=0.5).

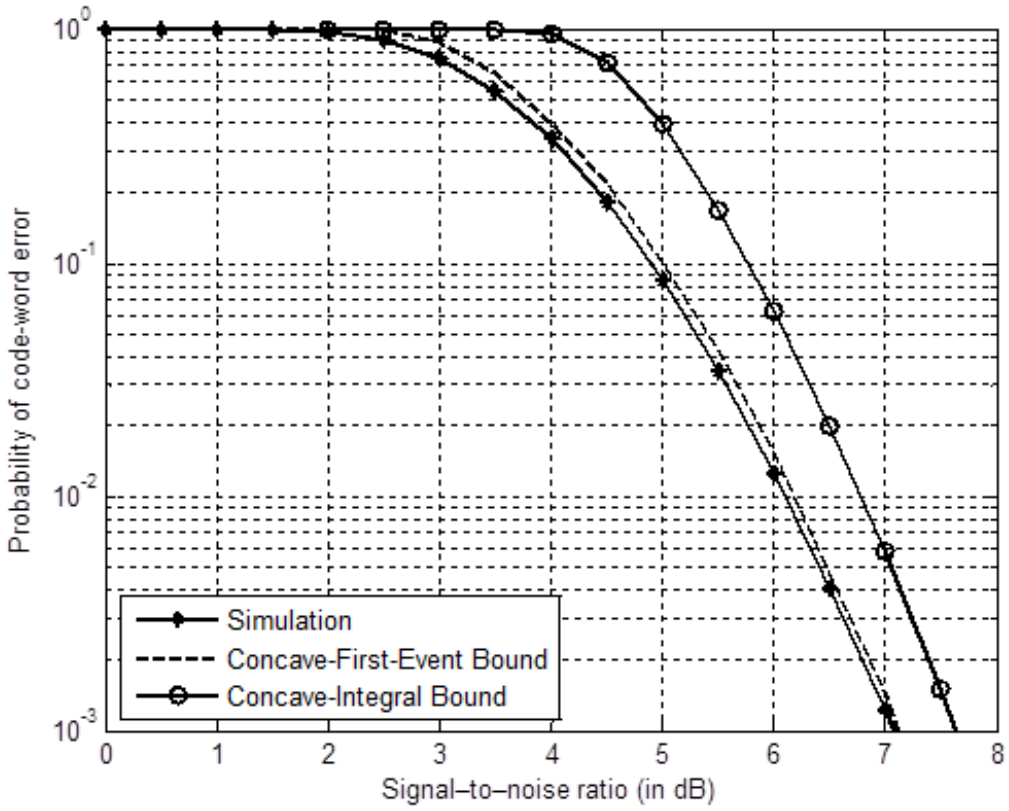

Figure 6.3: Comparison of bounds for memory-order-two encoder (ρ=1).

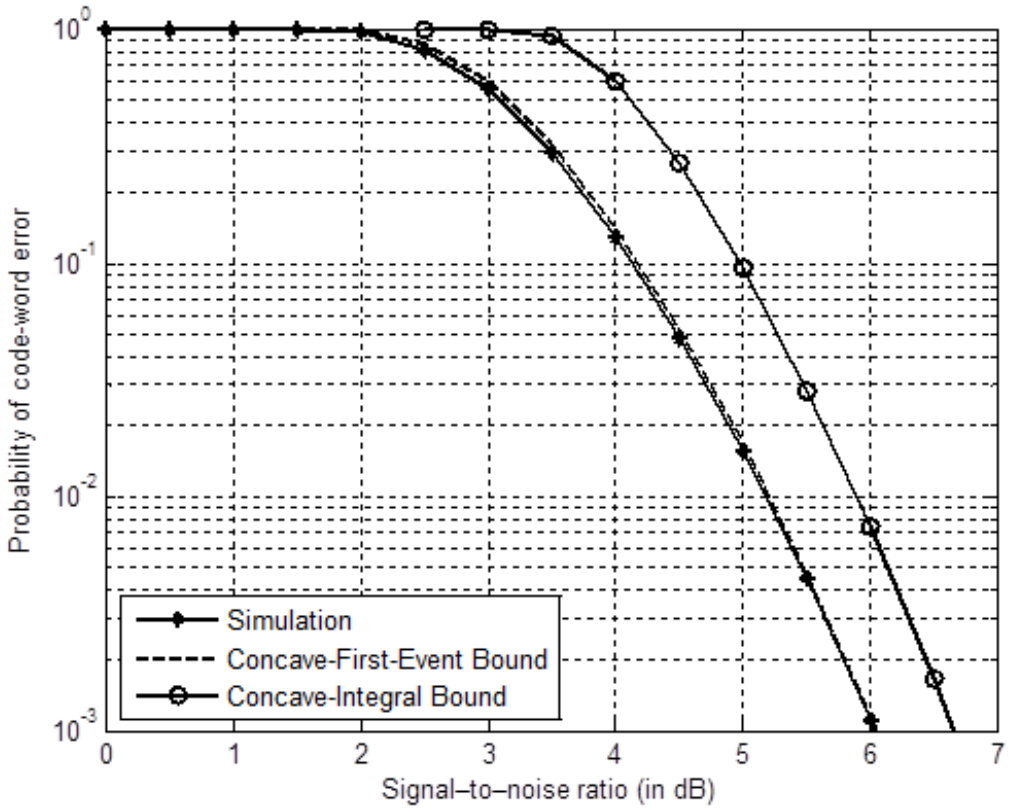

Figure 6.4: Comparison of bounds for memory-order-three encoder (ρ=0).

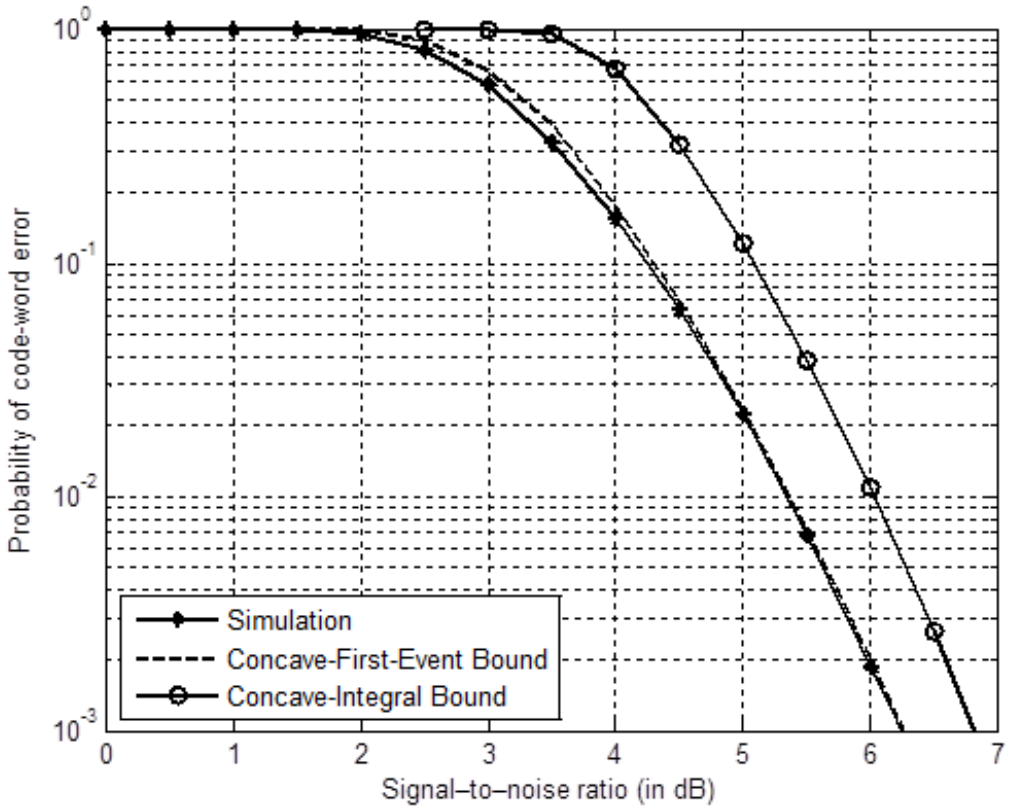

Figure 6.5: Comparison of bounds for memory-order-three encoder (ρ=0.5).

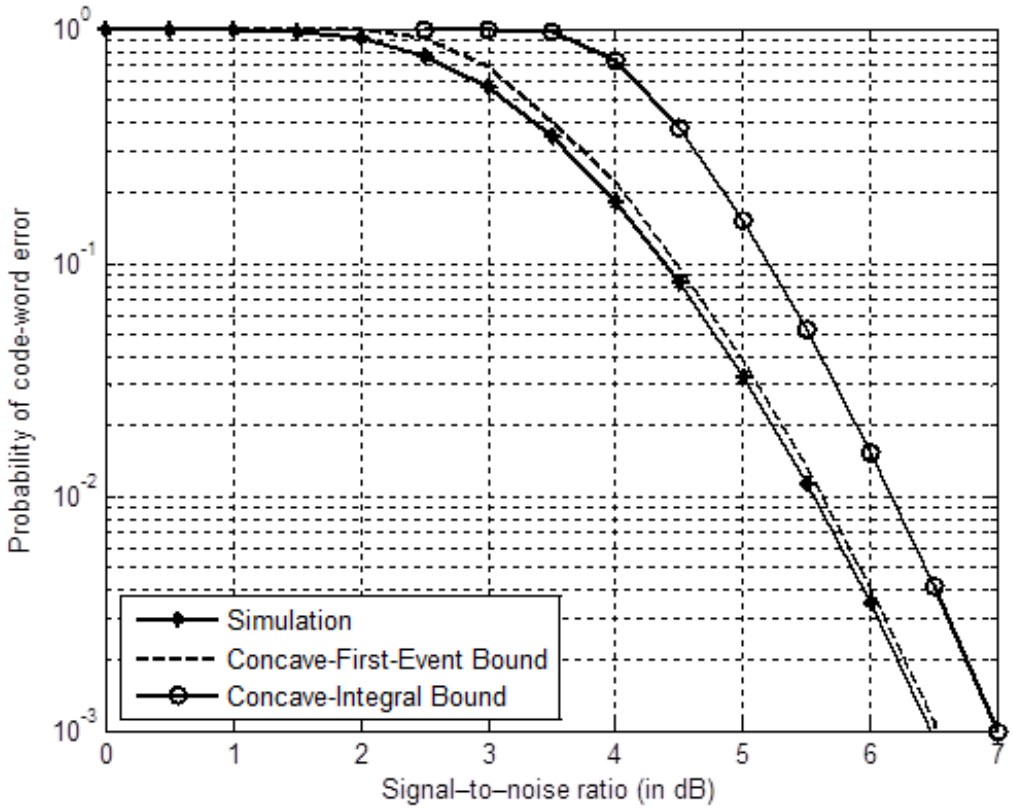

Figure 6.6: Comparison of bounds for memory-order-three encoder (ρ=1).

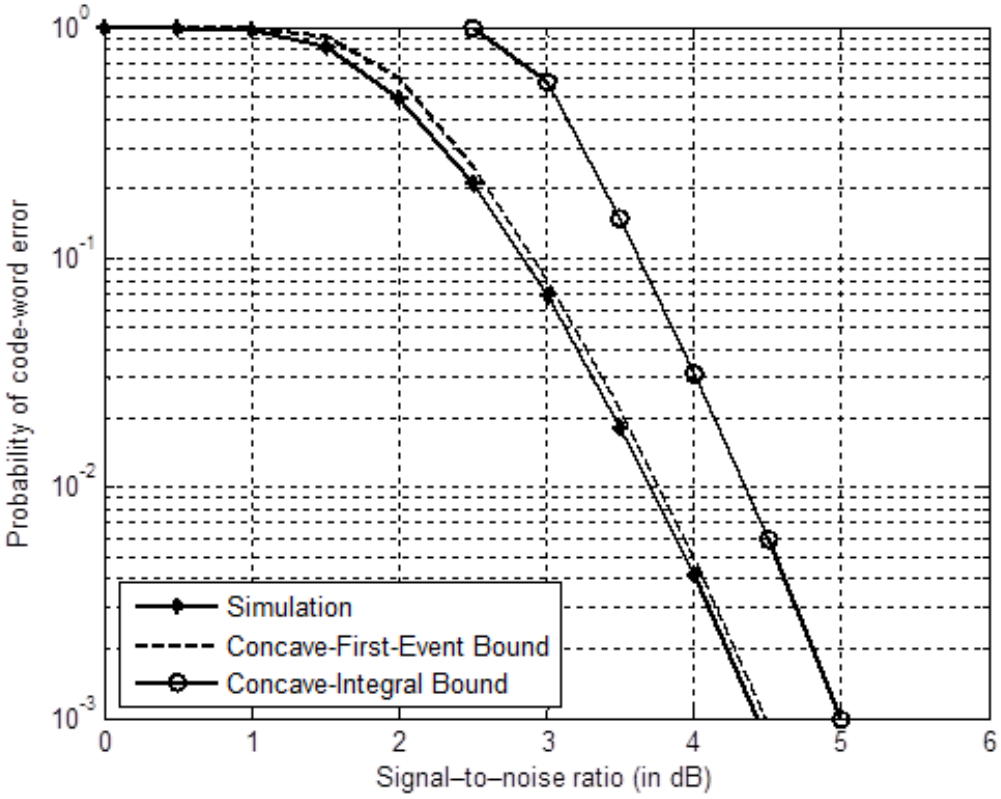

Figure 6.7: Comparison of bounds for NASA-standard encoder (ρ=0).

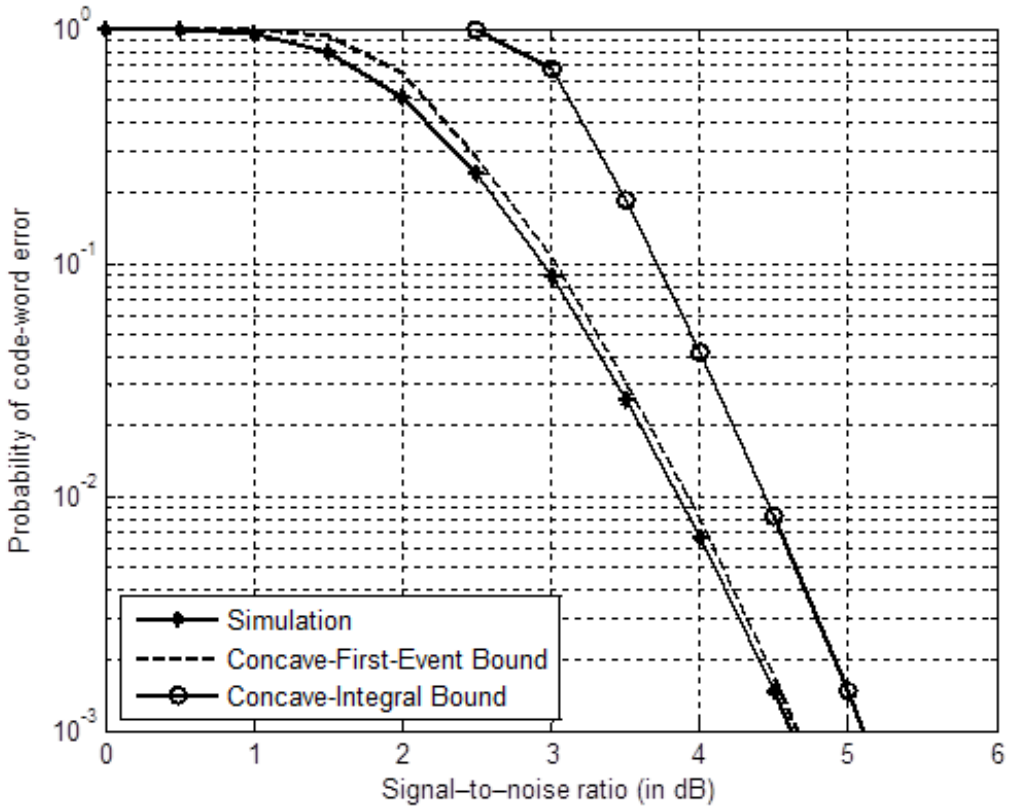

Figure 6.8: Comparison of bounds for NASA-standard encoder (ρ=0.5).

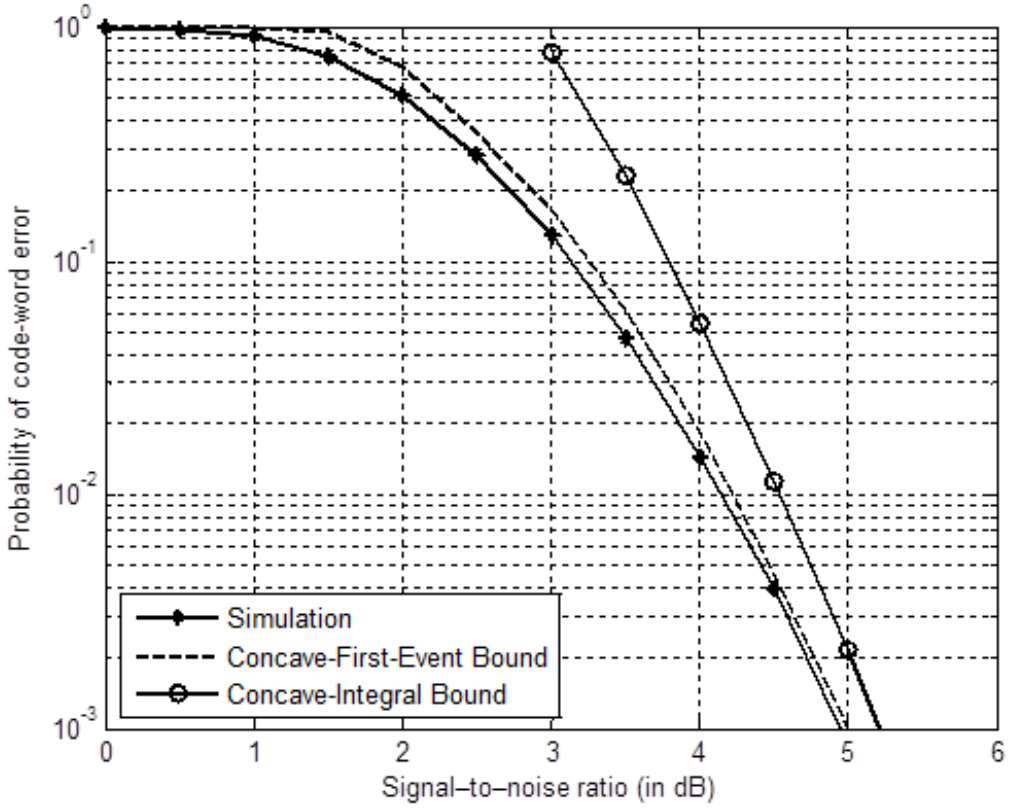

Figure 6.9: Comparison of bounds for NASA-standard encoder (ρ=1).

Chapter 7

Conclusion

The standard Gaussian approximation to multiple-access interference provides an accurate approximation to the performance of a communication system using convolutional coding, binary direct-sequence spread-spectrum modulation with quaternary spreading, and soft-decision Viterbi decoding. The first and second moments of interference terms in the receiver statistics are determined in the thesis using an approach similar to one used previously to determine the analogous moments for a system employing quaternary modulation with quaternary spreading. The moments of the interference terms provide the basis for a simulation-based approximation to the system performance and the concave-first-event bound and the concave-integral bound on the system performance.

Using several examples of convolutional codes and considering different multiple-access interference environments, it is shown in the thesis that the SGA yields a simulation-based probability of code-word error than is indistinguishable from the simulation-based probability of code-word error for actual system with multiple-access interference. The use of the SGA with the concave-first-event bound, which is a simulation-assisted closed-form bound, is shown to provide an approximation of the actual system's performance that is highly accurate. (The two are in agreement within 0.5 dB in all examples that are considered in the thesis and within 0.2 dB in most instances.) The SGA used in conjunction with the concave-integral bound provides an approximation of the actual system's performance that

is accurate to within 1.5 dB in all of the examples considered in the thesis, and its accuracy improves (especially for lower error probabilities) as the minimum Hamming distance of the convolutional code is increased.

The results in the thesis provide support for the use of the SGA to reduce the computational burden in the Monte Carlo simulation of the performance in a packet-radio network using direct-sequence spread-spectrum modulation and convolutional coding. Offline simulation of link performance for a Gaussian channel and different signal-to-noise-ratios can provide lookup tables of high accuracy for the network simulation even though the actual multiple-access interference in the network's links is non-Gaussian. Moreover, the analytical bounds based on the SGA can be used for either offline calculation or online calculation within the network simulation to provide accurate link outcomes with low computational burden.

Bibliography

[1] A. J. Viterbi, *CDMA: Principles of Spread Spectrum Communication*, Addison-Wesley, 1995.

[2] M. B. Pursley, "The role of spread spectrum in packet radio networks," *Proceedings of the IEEE*, vol. 75, pp. 116-134, Jan. 1987.

[3] Mohamed A. Landolsi and Wayne E. Stark, "On the Accuracy of Gaussian Approximations in the Error Analysis of DS-CDMA With OQPSK Modulation," *IEEE Transactions on Communications*, vol.50, pp. 2064 - 2071, Dec 2002.

[4] Shweta Tomar, "New Analytical Bounds on the Probability of Code-Word Error for Convolution Codes with Viterbi Decoding," M.S. Thesis, Clemson University, 2011.

[5] S. Lin and D. J. Costello Jr., *Error Control Coding*, Upper Saddle River, NJ: Pearson-Prentice Hall, 2004.

[6] J. S. Lehnert and M. B. Pursley, "Error probabilities for binary direct-sequence spread-spectrum communications with random signature sequences," *IEEE Trans. Commun.*, vol. COM-35, pp. 87-98, Jan. 1987.

[7] A. J. Viterbi, "Convolutional codes and their performance in communication systems," *IEEE Transactions on Communications*, vol. COM-19, pp. 751-772, Oct. 1971.

[8] D. Slepian, "The one-sided barrier problem for Gaussian noise," *Bell System Technical Journal*, vol. 41, pp. 463-501, 1962.

[9] Consultative Committee for Space Data Systems, "TM synchronization and channel coding - summary of concept and rationale," Green Book, vol. CCSDS, pp. 130.1-G-2, issue 2, Nov. 2012.

[10] I. M. Onyszchuk, "On the performance of convolutional codes," Ph.D. dissertation, California Institute of Technology, 1990.